

## Performance of Manganese and Antimony co-doping Tin Dioxide Anodes Prepared at Different Temperatures

Cairu Shao<sup>1,\*</sup>, Hongxing Ma<sup>1</sup>, Jianhua Zhang<sup>1</sup>, Yusi Jiang<sup>1</sup>, Huayue Cheng<sup>1</sup>, Xia Li<sup>2</sup> and Kaigui Zhu<sup>2</sup>

<sup>1</sup> Guangdong Research Institute of Rare-Metal, Guangzhou 510651, PR China

<sup>2</sup> Department of physics, Beihang University, Beijing 100191, PR China.

\*E-mail: [shaocairu@163.com](mailto:shaocairu@163.com)

Received: 6 August 2018 / Accepted: 27 September 2018 / Published: 30 November 2018

---

In this article, the titanium based Mn-Sb co-doping SnO<sub>2</sub> anodes (Ti/Mn-Sb-SnO<sub>2</sub>) prepared by the coating pyrolysis method at different annealing temperatures were investigated. The novel Ti/Mn-Sb-SnO<sub>2</sub> anodes did not only perform higher stability than the Ti/Sb-SnO<sub>2</sub> without Mn doping, but also exhibit superior capability of degrading phenol. The electrodes were characterized by X-ray diffraction (XRD), scanning electron microscopy (SEM) with energy dispersive X-Ray (EDX), polarization curve, chronopotentiometry, and phenol degradation simulation. Among all the samples, the Ti/Mn-Sb-SnO<sub>2</sub> electrode annealed at 550 °C performed the best catalytic stability. Moreover, the phenol removal efficiency of Ti/Mn-Sb-SnO<sub>2</sub> anode made at 600 °C almost reached 100% in 2h. To probe into the deep reason resulting in the better catalysis, the fluorescence spectrum method was applied to test the hydroxyl radicals produced on the surfaces of each electrodes in phenol oxidation. The results confirmed Mn-doping could promote the catalysis activities of Ti/Mn-Sb-SnO<sub>2</sub> electrodes.

---

**Keywords:** Dimensionally stable anodes; Antimony doped tin dioxide; Manganese; phenol degradation.

### 1. INTRODUCTION

Purification of wastewater has always been one of the crucial global challenges as the organic contaminants and hazardous pollutants from industrial productions have been causing serious environment and health problems. So far, numerous techniques have been employed in wastewater treatments, such as coagulation, adsorption, membrane separation, biological treatment, photocatalysis, and advanced oxidation processes (AOPs) [1-3]. As one kind of AOPs, the electrochemical catalysis has gained extensive attentions for its excellent elimination capability and variety of degradable pollutants [4, 5]. Dimensionally stable anodes (DSAs) are those electrodes coated with metal oxide on substrates, which are also called mixed metal oxide (MMO) electrodes, have been widely used in electrochemical

catalysis [6-9]. The performance of a DSA is significantly influenced by the electrode material [10], so selecting the electrode material is crucial for the efficiency of a DSA. Those electrodes with high oxygen evolution potential (OEP), long life, high catalysis activity, cheap price and low charge transfer resistance are required [11]. Several materials such as platinum (Pt) [12], boron-doped diamond (BDD) [13], and titanium-based metal oxides including iridium dioxide ( $\text{IrO}_2$ ) [14], ruthenium dioxide ( $\text{RuO}_2$ ) [15], lead dioxide ( $\text{PbO}_2$ ) [16], and antimony-doped tin oxide (ATO) [17] have been investigated in electrocatalytic oxidation. So far, it has been proven that only two electrode materials are capable of generating ozone with efficiencies over 20% at room temperature and using solutions that do not contain expensive fluorine-containing anions: they are BDD and Ti/Sb-SnO<sub>2</sub> [18]. Compared with BDD, it's obviously that Ti/Sb-SnO<sub>2</sub> has superiority in price. Although Ti/Sb-SnO<sub>2</sub> electrode has a good performance in electrocatalytic efficiency, the serious disadvantage is the poor stability seriously which limited its extensive application [19, 20].

Modifications of Ti/Sb-SnO<sub>2</sub> electrode by adding noble ion dopants or inserting interlayers can significantly improve the service life [21]. Correa-Lozano et al. [22] improved the accelerated lifetime of Ti/SnO<sub>2</sub>-Sb<sub>2</sub>O<sub>5</sub> anodes to 800 hours at current density of 100 mA·cm<sup>-2</sup> in 1 M H<sub>2</sub>SO<sub>4</sub> by depositing IrO<sub>2</sub> interlayer. Raúl et al. [23] found that the adding just small amounts of Pt and Ru could increase the accelerated lifetime up to 200 hours at 500 mA·cm<sup>-2</sup> current density in 1 M NaOH. Cui et al. [24] investigated the influence of doping rare earth elements Ce, Eu, Gd and Dy into the Ti/Sb-SnO<sub>2</sub> electrodes, finding that the Gd-doped Ti/Sb-SnO<sub>2</sub> electrode performed better durability and catalytic activity. Although the service lives of Ti/Sb-SnO<sub>2</sub> electrodes was extended, the oxygen evolution potentials of the electrodes were decreased and the cost increased at the same time. So to find cheaper and efficient dopants is still a hotspot in this field. Manganese is one of the most widely distributed elements in the crust. Laxmikanta et al. demonstrated that doping Mn into the antimony-tin oxide film may affect the crystallite size and band gap of SnO<sub>2</sub> crystal [25]. Kimura. H et al. [26] found out that Sn<sub>0.95</sub>Mn<sub>0.05</sub>O<sub>2</sub>:Sb film showed giant positive magneto-resistance as large as 60% at 5 K. However, the manganese and antimony co-doping titanium-based tin oxide electrodes have not been investigated systematically. In our previous work we had already introduced Mn-Sb co-doping SnO<sub>2</sub> anodes with different Mn doping concentrations [27]. To complete the investigation about Mn-Sb co-doping SnO<sub>2</sub> anodes, we studied the Ti/Mn-Sb-SnO<sub>2</sub> electrodes prepared at different annealing temperatures and their capabilities of degrading phenol. In the present research, we demonstrated the Mn-Sb co-doped SnO<sub>2</sub> anodes exhibited superior capability of degrading phenol. The phenol removal efficiency of Ti/Mn-Sb-SnO<sub>2</sub> anode prepared at 600 °C can reach nearly 100% in 2 h.

## 2. EXPERIMENT METHODS

We prepared Ti/Mn-Sb-SnO<sub>2</sub> electrodes by traditional coating pyrolysis method. The substrate for all electrodes were Ti plates with dimensions of 3×3 cm<sup>2</sup>. The Ti plates were firstly underwent sandblasting, then ultrasonic cleaned in deionized water, after that degreased in 40% sodium hydroxide at 90 °C for 2 h, and then etched in 10% oxalic acid at 95 °C for 1h followed by a thorough washing with deionized water and dried in nitrogen flow. The precursor solutions were a mixture of SnCl<sub>4</sub>·5H<sub>2</sub>O, Sb<sub>2</sub>O<sub>3</sub> and MnCl<sub>2</sub>·4H<sub>2</sub>O, in which the atomic ratio of Sn: Sb: Mn was at 50:3:3. alcohol and small amount of

concentrated hydrochloric acid was chosen as solvents. The precursor solutions were dripped on the substrates and dispersed uniformly, and then the electrodes were dried at 100 °C for 5 min and baked in the muffle furnace for 5 min at 450°C, 500°C, 550°C, and 600°C for comparisons. All the coating procedure were operated in the air atmosphere. After 20 times coating process, the electrodes were annealed for 1 h to be oxidized thoroughly.

The morphologies of Ti/Sb-SnO<sub>2</sub> and Ti/Mn-Sb-SnO<sub>2</sub> anodes were characterized by a Hitachi-S4800 field emission scanning electron microscopy (SEM) equipped with X-ray detector for energy dispersive X-Ray (EDX). The microstructures were measured by a Shimadzu-6000 X-ray diffraction analysis (XRD) using a diffractometer with Cu K $\alpha$  radiation ( $\lambda = 0.15406$  nm) and working at 30 kV / 40 mA. The diffraction patterns were collected in the range of  $2\theta = 20 - 80$  degree at a rate of 5 degree / min.

Electrochemical tests were carried out in a conventional three-electrode cell monitored by an electrochemical workstation (CHI-600E). The as-prepared electrodes and a platinum were employed as the working electrodes and counter electrode. Meanwhile, the Ag/AgCl electrode was selected as the reference electrode. The 1 M H<sub>2</sub>SO<sub>4</sub> solution was chosen as the electrolyte for all the electrochemical experiment.

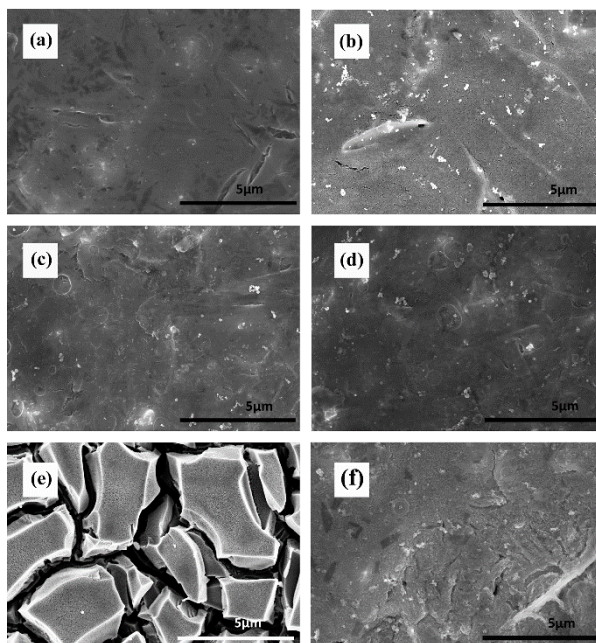
The phenol degradation experiments were carried out to dispose 60 mL 100 mg·L<sup>-1</sup> phenol in 0.25 M Na<sub>2</sub>SO<sub>4</sub> solution with a current density of 20 mA·cm<sup>-2</sup>. We used the prepared Ti/Mn-Sb-SnO<sub>2</sub> electrodes as the anode, and stainless steel as the cathode. The active area of anode was 2×3 cm<sup>2</sup> and the rest 1×3 cm<sup>2</sup> coating film was removed by polishing, all the active area was completely immersed in phenol solution. The phenol concentrations were examined by the standard 4-AAP spectrophotometric method (HJ 503-2009, China).

We chose terephthalic acid as the trapping agent to get hydroxyl radicals produced by the anode in oxidation process. Through checking the amount of the 2-hydroxy terephthalic acid by fluorescence spectrum we can compare the capacity of each electrode for producing hydroxyl radicals. Identical with the phenol degradation experiments, the active areas of anodes were still 2×3 cm<sup>2</sup> and the 1×1 cm<sup>2</sup> platinum plate was used as the cathode. The volume of electrolyte was 100 mL which included 0.5 mmol·L<sup>-1</sup> terephthalic acid and 0.25 mol·L<sup>-1</sup> Na<sub>2</sub>SO<sub>4</sub>. The current density was 10 mA·cm<sup>-2</sup>. We took out 2 mL electrolyte solution every 5 minutes and diluted the samples into 10 mL. The fluorescence excitation wavelength and the emission wavelength of 2-hydroxy terephthalic acid were 315 nm and 425 nm, respectively.

### 3. RESULTS AND DISCUSSION

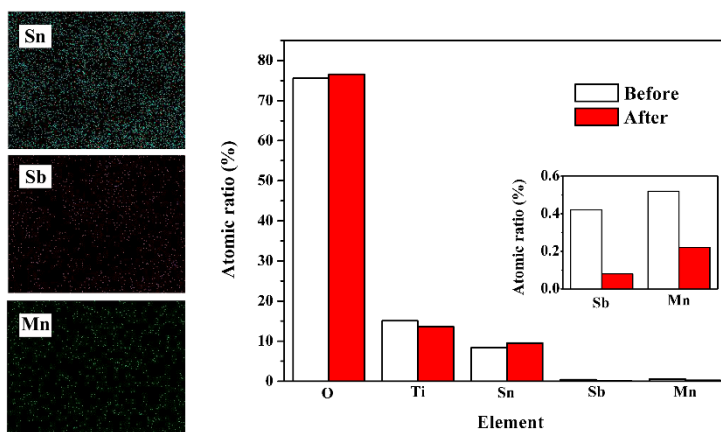
Figure 1 (a), (b), (c) and (d) reveal the scanning electron microscopy (SEM) images of the Ti/Mn-Sb-SnO<sub>2</sub> electrodes prepared at different annealing temperatures. As can be seen, all the Mn-Sb co-doping electrodes showed significantly promoted morphologies which have fewer cracks and smoother surfaces compared with the Ti/Sb-SnO<sub>2</sub> anode shown in Fig.1(e). The cracked-mud morphology was recognized as the result of calcination[28], It means introducing manganese into the Sb-SnO<sub>2</sub> can enhance the thermal stress resistance of coating and lead to a more compact morphological structure.

Since previous study had already demonstrated that the electrodes with dense and smooth surfaces were difficult to be damaged, and cracks may help the acidic solution to corrode the Ti substrate and facilitate the growth of  $\text{TiO}_2$  passivation layer[29-30]. Furthermore, the subsequent accelerated life test confirmed this inference. Fig.1 (f) shows the morphology of the deactivated  $\text{Ti/Mn-Sb-SnO}_2$  electrode which was prepared at  $550^\circ\text{C}$ . In contrast with that shown in Fig.1 (c), the electrode after the accelerated life test has more cracks than the as-prepared one, and coating shedding appeared in some places. It's probably because the electrolyte damaged the catalytic coating during the catalytic process. Then the electrolyte permeated these cracks and accelerated the attenuation of servicelife.

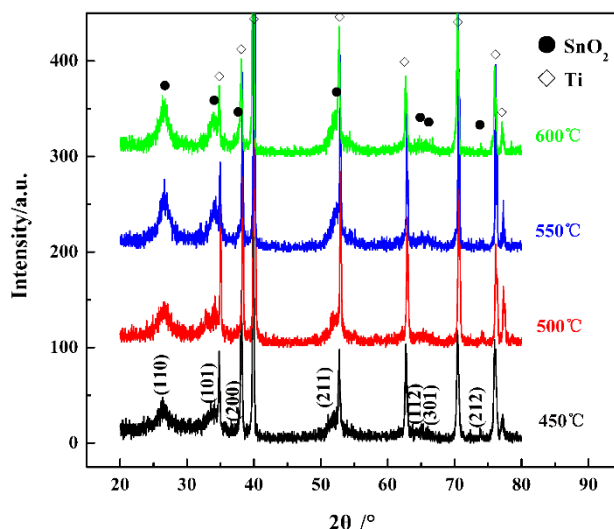


**Figure 1.** SEM images of (a)  $\text{Ti/Mn-Sb-SnO}_2$  electrodes prepared at  $450^\circ\text{C}$ , (b)  $500^\circ\text{C}$ , (c)  $550^\circ\text{C}$ , (d)  $600^\circ\text{C}$ , (e)  $\text{Ti/Sb-SnO}_2$  electrode, (f) deactivated  $\text{Ti/Mn-Sb-SnO}_2$  electrodes prepared at  $550^\circ\text{C}$ .

The left three images in Fig.2 are element-mappings of Sn, Sb and Mn on the electrode surface, which were used for analyzing the elements distribution. We found that the elements of Sn, Sb, and Mn were all uniformly distributed on the Ti plates. The histogram at the right of Fig.2 exhibits the atomic ratio before and after the accelerated life test obtained by EDX analysis. The white columns stand for the as-prepared  $\text{Ti/Mn-Sb-SnO}_2$  anode and red columns represent the deactivated electrode. Except oxygen and tin atomic ratio increased, all other elements decreased slightly after the use. We thought the increase of oxygen atomic ratio is due to the partial oxidation of titanium substrate. Since a semiconductor is sensitive in conductivity to its dopants. Even small amount dopants could determine the properties of materials. From the enlarged view about Sb and Mn elements, we could find the atomic ratios of dopants decrease significantly after accelerated life test. The decrease of dopants content may result in attenuation of coating conductivity. So we believe the deactivated mechanism of  $\text{Ti/Mn-Sb-SnO}_2$  anode is very complex. The formation of  $\text{TiO}_2$  passivation layer is only one of the reasons.

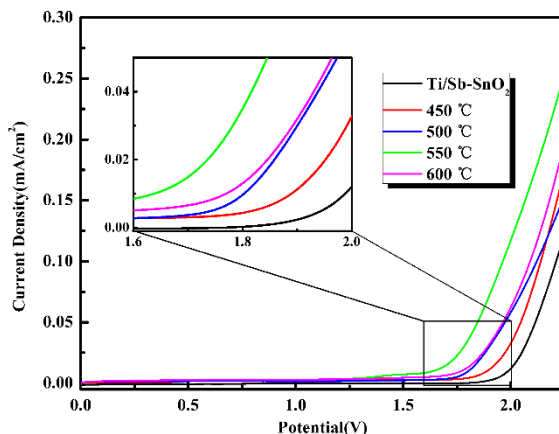


**Figure 2.** Element-mapping for the Ti/Mn-Sb-SnO<sub>2</sub> electrode prepared at 550°C, and atomic ratio of elements on the Ti/Mn-Sb-SnO<sub>2</sub> electrode surface before and after accelerated life test.



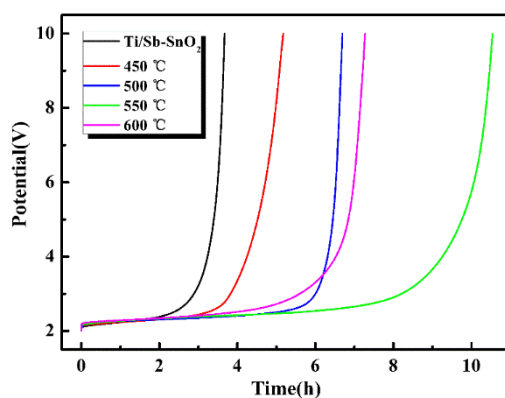
**Figure 3.** X-Ray diffractograms of Ti/Mn-Sb-SnO<sub>2</sub> electrodes made at different temperatures.

Fig.3 reveals the XRD patterns of the Ti/Mn-Sb-SnO<sub>2</sub> electrodes prepared at different annealing temperatures. By comparing with the standard PDF card, we can find there were only diffraction peaks of rutile-type SnO<sub>2</sub> (PDF#41-1445) and Ti (PDF#44-1294). Those spiculate peaks in Fig.3 were related to Ti substrate. This is because the rough titanium substrate has some bumps that will not be covered by the coating. As for the coating has poor crystallinity, peaks corresponding to dopant phases could not be identified. Through comparing the (110) crystal face of SnO<sub>2</sub> prepared at 450°C, 500°C, 550°C. We can clearly observe the peak intensities grow up gradually as the annealing temperature increasing. It means higher annealing temperature results in better crystallinities. Furthermore, we calculated the crystallinity of SnO<sub>2</sub> coating, and found the Ti/Mn-Sb-SnO<sub>2</sub> electrodes made at 550°C and 600°C had the better crystallinity than that made at 450°C and 500°C, which were 80.62%, 80.27%, 75.81% and 78.04%, respectively. This result is similar with that of the Ti/ Sb-SnO<sub>2</sub> electrodes [31].



**Figure 4.** Linear sweep voltammetry curves of Ti/Sb-SnO<sub>2</sub> electrode and Ti/Mn-Sb-SnO<sub>2</sub> electrodes prepared at different temperatures. The tests were performed in 1 M H<sub>2</sub>SO<sub>4</sub> solution with scanning rate of 100mV/s.

Fig.4 shows the linear sweep voltammetry (LSV) curves of Ti/Sb-SnO<sub>2</sub> electrode and Ti/Mn-Sb-SnO<sub>2</sub> electrodes made at different temperatures. From the picture, we can read out the oxygen evolution overpotential of Ti/Sb-SnO<sub>2</sub> is about 2.0 V, this value is consistent with the previous reports[32]. Meanwhile, the oxygen evolution overpotential of Ti/Mn-Sb-SnO<sub>2</sub> is about 1.9 V at 450 °C, 1.7 V at 500 °C, 1.6 V at 550 °C, and 1.8 V at 600 °C, respectively.



**Figure 5.** Accelerated service life curves of Ti/Sb-SnO<sub>2</sub> electrode and Ti/Mn-Sb-SnO<sub>2</sub> electrodes prepared at different temperatures. The test performed in 1 M H<sub>2</sub>SO<sub>4</sub> solution with anodic current density of 100mA/cm<sup>2</sup>.

As we all know, the electrodes with higher oxygen evolution overpotential conduct lower side reaction and better current efficiency, which would benefit the electrocatalytic oxidation efficiency of organic pollutants. The degradation of organic pollutant molecules needs to provide a initiate potential, and the oxygen evolution overpotential of electrode should higher than the initiate potential. So that more electricity could be used to electrolyze organic pollutant. The oxygen evolution overpotentials of electrode with Mn doping were lower than those without Mn. Maybe this is because Mn atoms enter the

SnO<sub>2</sub> crystal and result in a better conductivity for electrode. As discussed in previous work[33], the oxidation potential corresponding to the oxygen evolution overpotential depends on the strength of interaction between electrodes and hydroxyl radicals. The stronger electrode-hydroxyl radical interaction on the surface of electrodes bring a lower oxidation potential. So it can be deduced that the introduction of Mn results in a stronger interaction between electrode and hydroxyl radicals.

The stabilities of Ti/Mn-Sb-SnO<sub>2</sub> electrodes were investigated through chronopotentiometry, and Fig.5 displays the results of test. We can easily find the lives of Ti/Mn-Sb-SnO<sub>2</sub> electrodes were all longer than that of the Ti/Sb-SnO<sub>2</sub> electrode. Our previous work already demonstrated the stability of Ti/Mn-Sb-SnO<sub>2</sub> electrodes with different Mn concentrations were all better than that of Ti/Sb-SnO<sub>2</sub>. Many researches have studied the stability of Ti/Sb-SnO<sub>2</sub> electrode[34, 35], all of those reports reveal Ti/Sb-SnO<sub>2</sub> electrode without any modification have poor servicelife. Herein the accelerated life of the pure antimony doped tin dioxide electrode was only 3 h in 1 M H<sub>2</sub>SO<sub>4</sub> solution with anodic current density of 100mA/cm<sup>2</sup>, but that of Ti/Mn-Sb-SnO<sub>2</sub> electrode which was made at 550°C reached 10 h under the same test conditions. The accelerated life of Mn and Sb co-doping SnO<sub>2</sub> anodes made at 500°C and 600°C all came up to 6 h. So we believed that the electrode stability can be enhanced by introducing Mn into the Ti/Sb-SnO<sub>2</sub>. This result is potentially helpful for expanding the applications of titanium base tin dioxide electrodes.

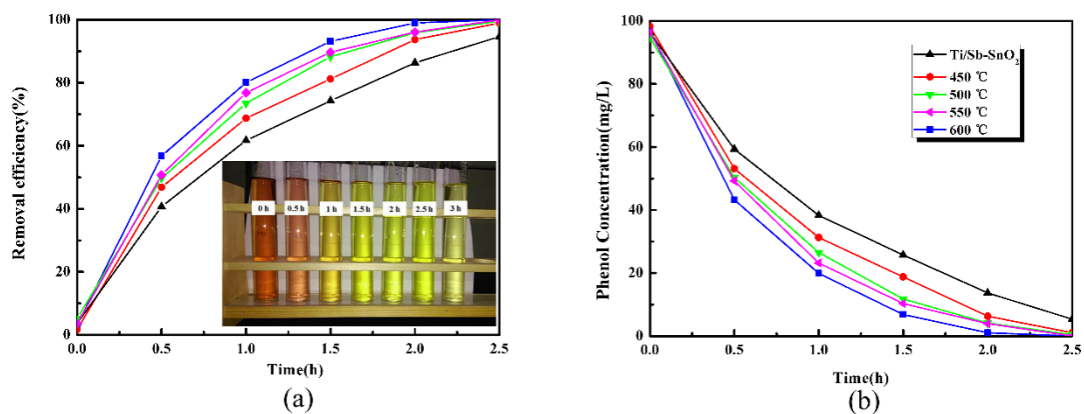


**Figure 6.** Phenol degradation curves of Ti/Sb-SnO<sub>2</sub> electrode and different Ti/Mn-Sb-SnO<sub>2</sub> electrodes in 60 mL 0.25 M Na<sub>2</sub>SO<sub>4</sub> electrolyte. The initial concentration of phenol is 100 mg·L<sup>-1</sup>, constant current density=20 mA·cm<sup>-2</sup>.

Phenol was chosen as the object pollutant of the electrocatalytic degradation process. The degradation curves and removal efficiencies are shown in Fig.6. The digital picture in Fig.6 exhibits the color change after adding 4-aminoantipyrine and potassium ferricyanide into the samples that taken at different time in phenol degradation using the Ti/Mn-Sb-SnO<sub>2</sub> electrode (600°C). The concentration of phenol decreased to less than 10 mg/L after nearly 2.5 h by using the Ti/Sb-SnO<sub>2</sub> without Mn doping as electrocatalysis anode, but it only took 2h to achieve the same removal efficiency by using Mn-Sb co-doping SnO<sub>2</sub> electrodes. Furthermore, the removal efficiency of Ti/Mn-Sb-SnO<sub>2</sub> electrode prepared at 600°C almost reached 100% in 2h. We list some other phenol removal research results in Table 1. Under

different conditions, the phenol removal efficiencies can not be compared directly. Because there are many factors that may affect the performance of electrode, such as initial concentration and volume of phenol, current density, space between anode and cathode. No matter under what kind of condition, the Ti/Sb-SnO<sub>2</sub> electrode always exhibit high removal efficiency with phenol. We thought the reasons why Mn-Sb co-doping can improve the catalytic activity of electrodes were very complex. Due to the Mn<sub>2</sub>O<sub>3</sub> (Mn<sup>3+</sup>) was considered as the most active phase for water splitting, which leads to the indirect oxidation of phenol through a reaction with O<sub>3</sub> [39-41]. While MnO<sub>2</sub> (Mn<sup>4+</sup>) is more active for phenol oxidation or in the heterogeneous catalysis, because of its ability to degrade organic molecules by producing hydroxyl radicals ( $\bullet$ OH). Due to the special *d* electrical structure, most kinds of manganese oxides are the non-equilibrium phases and have many crystal defects and lattice distortions. The ions in whether plane defects or point defects all have high chemical activities. So maybe the ions in defects also provided chemical activation energy and involved in the phenol degradation reactions.

**Table 1.** Phenol removal data of some other researches and this work.

Electrode Type	Experiment Condition		Time
	Initial Concentration and Volume of Phenol / Current Density / Anodic Area /Distance between Anode and Cathode		
Ti/Sb-SnO <sub>2</sub>	100 mg/L, 60 mL , 20 mA/cm <sup>2</sup> , 2×3 cm <sup>2</sup> , 10mm		>2.5h <sup>[this work]</sup>
Ti/Mn-Sb-SnO <sub>2</sub>	100 mg/L, 60 mL , 20 mA/cm <sup>2</sup> , 2×3 cm <sup>2</sup> , 10mm		2h <sup>[this work]</sup>
Ti/SnO <sub>2</sub> -Sb	490 mg/L, 100 mL, 20 mA/cm <sup>2</sup> , 2×3 cm <sup>2</sup> , 8 mm		5h <sup>[36]</sup>
Ti/RuO <sub>2</sub>	490 mg/L, 100 mL, 20 mA/cm <sup>2</sup> , 2×3 cm <sup>2</sup> , 8 mm		36h <sup>[36]</sup>
Pt	490 mg/L, 100 mL, 20 mA/cm <sup>2</sup> , 2×3 cm <sup>2</sup> , 8 mm		18h <sup>[36]</sup>
Ti/SnO <sub>2</sub> -Sb	500 mg/L, 100 mL, 30 mA/cm <sup>2</sup> , 3×4 cm <sup>2</sup> , 15 mm		>2.5h <sup>[37]</sup>
Ti/SnO <sub>2</sub> -Sb-La	500 mg/L, 100 mL, 30 mA/cm <sup>2</sup> , 3×4 cm <sup>2</sup> , 15 mm		2h <sup>[37]</sup>
Ti/SnO <sub>2</sub> -Sb-Ru	500 mg/L, 100 mL, 30 mA/cm <sup>2</sup> , 3×4 cm <sup>2</sup> , 15 mm		2.5h <sup>[37]</sup>
Ti/SnO <sub>2</sub> -Sb-Gd	100 mg/L, 80 mL, 20 mA/cm <sup>2</sup> , 2×3 cm <sup>2</sup> , 15 mm		>3h <sup>[38]</sup>

It is believed that the catalytic activity of an anode strongly depends on the capacity of producing hydroxyl radicals. To find the reason why the Ti/Mn-Sb-SnO<sub>2</sub> electrode can degrade phenol faster than the Ti/Sb-SnO<sub>2</sub> electrode, we checked the amount of hydroxyl radicals generated in the oxidation process by fluorescence spectrum. The experiment details has already been described in the method section. The symbols in Fig.7 represent the fluorescence intensities of the 2-hydroxy terephthalic acid in samples which were taken at different time of each anodic oxidation process. Fitting the fluorescence intensity data into lines, we can get the slopes of fitted lines which were exactly the hydroxyl radical generation rates of each anode. In equation (1),  $\delta$  represents the hydroxyl radical generation rate. Table.1 displays the  $\delta$  values of different electrodes.

$$\frac{d(\bullet OH)}{dt} = \delta t \quad (1)$$

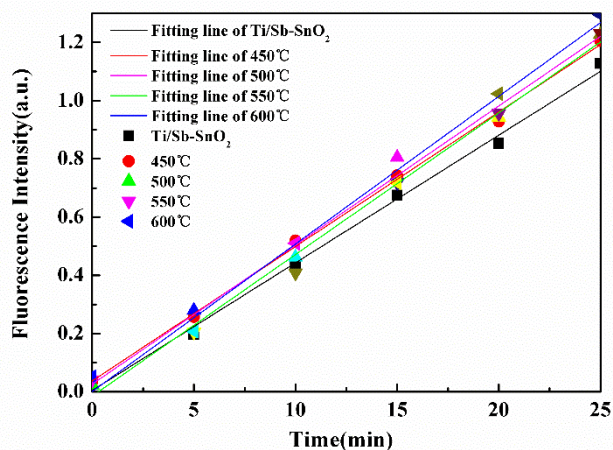


**Figure 7.** Fluorescence intensities of 2-hydroxy terephthalic acid taken from different anodic oxidation processes at different time and the fitted lines of each set of fluorescence intensities data.

**Table 2.** The hydroxyl radical generation rates of different electrodes.

Electrode	$\delta$ (min <sup>-1</sup> )
Ti/Sb-SnO <sub>2</sub>	0.04385
Ti/Mn-Sb-SnO <sub>2</sub> (450°C)	0.04621
Ti/Mn-Sb-SnO <sub>2</sub> (500°C)	0.04777
Ti/Mn-Sb-SnO <sub>2</sub> (550°C)	0.04865
Ti/Mn-Sb-SnO <sub>2</sub> (600°C)	0.05069

From Table 2 we can clearly see the  $\delta$  values are all positive. It confirm the generation rate of hydroxyl radical is proportional to the time, which is consistent with the zero order kinetics. We can also find the  $\delta$  values of all the Ti/Mn-Sb-SnO<sub>2</sub> electrodes are higher than that of Ti/Sb-SnO<sub>2</sub>, which means the Ti/Mn-Sb-SnO<sub>2</sub> electrodes have better hydroxyl radical delivery efficiency than Ti/Sb-SnO<sub>2</sub>. That was the immediate reason leading to the faster catalysis activities of Ti/Mn-Sb-SnO<sub>2</sub> anodes for phenol degradation. As far as the effect of the temperature ramp during calcination was concerned, Ti/Mn-Sb-SnO<sub>2</sub> electrode made at 600°C performed the best capacity for generating hydroxyl radicals. We deduced the reason of this phenomenon was because the higher annealing temperature made more oxygen vacancy escaping out. With the decreasing of oxygen vacancy, more oxygen atom would enter into the crystalline when the metal oxide formation. So the manganese maybe more likely oxidized as Mn<sup>4+</sup> ions while in the higher temperature calcination. As already discussed in phenol degradation section, the Mn<sup>4+</sup> ions have more activities for phenol than Mn<sup>3+</sup>, so the electrode made at 600 °C had the best catalysis efficiency in this work. Some reasearchers demonstrated that the Mn-O binding energy played a predominant role in the catalytic performance of MnO<sub>2</sub>[42]. The Mn-O bond would enhanced with the annealing temperature increasing, and which was also good for the phenol removal.

#### 4. CONCLUSIONS

The Ti/Mn-Sb-SnO<sub>2</sub> electrodes were successfully fabricated by coating pyrolysis method at different annealing temperatures. We used X-ray diffraction and scanning electron microscopy to analyze the crystal and microscopic structures of electrodes. The Ti/Mn-Sb-SnO<sub>2</sub> electrodes had more compact surfaces than the Ti/Sb-SnO<sub>2</sub> electrodes without Mn doping. Furthermore, the accelerated service life tests, phenol degradation tests and the hydroxyl radical tests were carried out to examine the electrochemical properties of Ti/Mn-Sb-SnO<sub>2</sub> electrodes, the results revealed that Mn doped Ti/Sb-SnO<sub>2</sub> electrodes not only perform longer accelerated life than the Ti/Sb-SnO<sub>2</sub> electrode without Mn, but also have better catalytic activity to phenol. At present, in industrial production, noble metals are usually used as dopants in Ti/Sb-SnO<sub>2</sub> electrodes to improve the stabilities. Manganese is widely distributed in nature and has a much cheaper price. Using manganese as dopant can largely reduce the cost of production. We believe that maybe manganese and antimony co-doping tin dioxide can be widely used in the future.

#### ACKNOWLEDGEMENTS

This work was supported by the Special Program on Science and Technology Development of Guangdong Province (Grant No.2017A070702012, Grant No.2017A070701022), and the GDAS' Project of Science and Technology Development ( Grant No.2017GDASCX-0110, Grant No.2018GDASCX-0937).

#### References

1. Carlos A. Martínez-Huitle and Sergio Ferroa, *Chem. Soc. Rev.*, 35 (2006) 1324.
2. J. C. Underwood, R. W. Harvey, D. W. Metge, D. A. Repert, L. K. Baumgartner, R. L. Simth, T. M. Roane and L. B. Barber, *Environ. Sci. Technol.*, 45 (2011) 3096.
3. Qiushi Yin, Jeffrey Miles Tan, Claire Besson, Yurii V. Geletii, Djamaladdin G. Musaev, Aleksey E. Kuznetsov, Zhen Luo, Ken I. Hardcastle and Craig L. Hill. *Science*, 328 (2010) 342.
4. Han Yu, Ya Li, Min Zhao, Heng Dong, Hongbing Yu, Sihui Zhan and Linus Zhang, *Catal. Today*, 258 (2015) 156.
5. Soonhyun Kim, Sung Kyu Choi, Bok Young Yoon, Sang Kyoo Lim and Hyunwoong Park, *Appl. Catal B-Environ.*, 97 (2010) 135.
6. Li Xu, Ming Li, Wei Xu, *Electrochim. Acta*, 166 (2015) 64.
7. Qiongfang Zhuo, Shubo Deng, Bo Yang, Jun Huang and Gang Yu, *Environ. Sci. Technol.*, 45 (2011) 2973.
8. So Young Yang, Dongseog Kim and Hyunwoong Park, *Environ. Sci. Technol.*, 48 (2014) 2877.
9. Aqing Chen, Xudong Zhu, Junhua Xi, Haiying Qin and Zhenguo Ji, *J. Alloy. Compd.*, 683 (2016) 501.
10. Guoping Wang, Lei Zhang, and Jiujun Zhang, *Chem. Soc. Rev.*, 41 (2012) 797.
11. Tao Wu, Guohua Zhao, Yanzhu Lei and Peiqiang Li, *J. Phys. Chem. C.*, 115 (2011) 3888.
12. F. Montilla, E. Morallon and J. L. Vazquez, *Electrochim. Acta*, 47 (2002) 4399.
13. Qiongfang Zhuo, Shubo Deng, Bo Yang, Jun Huang, Bin Wang, Tingting Zhang and Gang Yu, *Electrochim. Acta*, 77 (2012) 17.
14. S. Fierro, L. Ouattara, E. H. Calderon, E. Passas-Lagos, H. Baltruschat and C. Comminellis, *Electrochim. Acta*, 54 (2009) 2053.
15. Aleksandra Perek-Dlugosz, Adam Socha, Marek Socha, Jacek Rynkowski, *Electrocatalysis*, 6

- (2015) 563.
16. Yuan Liu and Huiling Liu, *Electrochim. Acta*, 53 (2008) 5077.
  17. Dan Shao, Xiaoliang Li, Hao Xu and Wei Yan, *RSC Adv.*, 4 (2014) 21230.
  18. Paul Andrew Christensen, Khalid Zakaria Henriette Christensen and Taner Yonar. *J. Electrochem. Soc.*, 160 (2013) 405.
  19. F. Montilla, E. Moralloín, A. D. Battisti, A. Benedetti, H. Yamashita and J. L. Vázquez, *J. Phys. Chem. B*, 108 (2004) 15976.
  20. Tigang Duan, Ye Chen, Qing Wen and Ying Duan, *RSC Adv.*, 5 (2015) 19601.
  21. Guo Li, Yunhai Wang and Qingyun Chen, *J. Solid. State. Electrochem.*, 17 (2013) 1303.
  22. B. Correa-Lozano, C. Comninellis and A. De Battisti, *J. Appl. Electrochem.*, 27 (1997) 970.
  23. Raúl Berenguer, Juan Manuel Sieben, César Quijada, and Emilia Morallón, *ACS Appl. Mater. Inter.*, 6 (2014) 22778.
  24. Yuhong Cui, Yujie Feng and Zhengqian Liu, *Electrochim. Acta*, 54 (2009) 4903.
  25. Laxmikanta Dua and Prasanta K. Biswas, *Appl. Surf. Sci.*, 280 (2013) 33.
  26. H. Kimura, T. Fukumura, M. Kawasaki, K. Inaba, T. Hasegawa, and H. Koinuma, *Appl. Phys. Lett.*, 80 (2002) 94.
  27. Cairu Shao, Aqing Chen, Bo Yan, Qingyi Shao and Kaigui Zhu, *J. Electroanal. Chem.*, 778 (2016) 7.
  28. Andrea Massa, Simelys Hernandez, Simone Ansaloni, Micaela Castellino, Nunzio Russo, Debora Fino, *Electrochim. Acta*, 273 (2018) 53.
  29. D. Santos, A. Lopes, M. J. Pacheco, A. Gomes, and L. Ciríaco, *J. Electrochem. Soc.*, 161 (2014) 564.
  30. M. Abbasi, J. Bäckström and A. Cornell, *J. Electrochem. Soc.*, 165 (2018) H568.
  31. Hilal Köse, Şeyma Karaal, Ali Osman Aydin, Hatem Akbulut, *Mat. Sci. Semicon. Proc.*, 38 (2015) 412.
  32. Kun Yang, Yuyu Liu and Jinli Qiao, *Sep. Purif. Technol.*, 189 (2017) 459.
  33. V. Smith De Sucre and A. P. Watkinson, *Can. J. Chem. Eng.*, 59 (1981) 52.
  34. Xueming Chen and Guohua Chen, *Electrochim. Acta*, 50 (2005) 4155.
  35. Xusong Qin, Furong Gao and Guohua Chen, *J. Electroanal. Chem.*, 40 (2010) 1797.
  36. Xiaoyan Li, Yuhong Cui, Yujie Feng, Zhaoming Xie, Jidong Gu, *Water Res.*, 39 (2005) 1972.
  37. Haiqing Xu, Aiping Li, Qi Qi, Wei Jiang and Yueming Sun, *Korean J. Chem. Eng.*, 29 (2012) 1178.
  38. Yujie Feng, Yuhong Cui, Bruce Logan, Zhengqian Liu, *Chemosphere*, 70 (2008) 1629.
  39. Alejandra Ramírez, Philipp Hillebrand, Diana Stellmach, Matthias M. May, Peter Bogdanoff, and Sebastian Fiechter, *J. Phys. Chem. C*, 118 (2014) 14073.
  40. Andrea Massa, Simelys Hernández, Andrea Lamberti, Camilla Galletti, Nunzio Russo, Debora Fino, *Appl. Catal B-Environ.*, 203 (2017) 270.
  41. Toshihiro Takashima, Kazuhito Hashimoto and Ryuhei Nakamura, *J. Am. Chem. Soc.*, 134 (2012) 18153.
  42. Ming Sun, Bang Lan, Ting Lin, Gao Cheng, Fei Ye, Lin Yu, Xiaoling Cheng and Xiaoying Zheng, *Cryst. Eng. Comm.*, 15 (2013) 7010.